

# Dielectric Behavior Characterization of a Fibrous-ZnO/PVDF Nanocomposite

Canan Dagdeviren, Melih Papila

Sabancı University, Faculty of Engineering and Natural Sciences, Material Science and Engineering, Tuzla, Istanbul 34956, Turkey

**This study is focused on forming a fibrous-zinc oxide/polyvinylidene fluoride (ZnO/PVDF) nanocomposite and characterizing its dielectric behavior. The nanocomposite is prepared in two steps. First, a network of nano-scale diameter ZnO fibers is produced by sintering electrospun PVA/Zinc Acetate fibers. Second, the ZnO fibrous nonwoven mat is sandwiched between two PVDF thermoplastic polymer films by hot-press casting. Scanning electron microscope images of the nanocomposite show that hot-press casting of the fibrous-ZnO network breaks the network up into short fibers. The in-plane distribution of the ZnO fillers (i.e., the short fibers) in the PVDF matrix appears to comply with that of the pristine ZnO fibers before hot-pressing, indicating that the fillers remain well-dispersed in the polymer matrix. To the authors' knowledge, the work reported herein is the first demonstration of the use of electrospinning to secure the dispersion and distribution of a network of inorganic fillers. Moreover, processing a fibrous-ZnO/PVDF flexible composite as described in this report would facilitate material handling and enable dielectric property measurement, in contrast to that on a fibrous mat of pure ZnO. Because of the high surface area of the short ZnO fibers and their polycrystalline structure, interfacial polarization is pronounced in the nanocomposite film. The dielectric constant is enhanced significantly-up to a factor of 10 at low frequencies compared to the dielectric constant of constituent materials (both bulk ZnO and PVDF), and up to a factor of two compared to a bulk-ZnO/PVDF composite. POLYM. COMPOS., 31:1003-1010, 2010. © 2009 Society of Plastics Engineers**

## INTRODUCTION

Zinc oxide (ZnO) is a technologically attractive material because of its potential for sensor applications [1, 2] enabled by catalysis [3], optical emission [4, 5], piezoelectric transduction and actuation [6–8]. The wide array

of nanostructures producible broadens the appeal for their incorporation into functional composites. Individual ZnO nanobelts, for instance, were produced and measurements by piezoresponse force microscopy revealed promising results for the future of ZnO in nano-sensors and nano-actuators industry [9]. Specifically, the effective piezoelectric coefficient was reported to impart an increase, attributed to the nano-scale structure, by more than a factor of two.

For producing ZnO nanostructures, a variety of physical or chemical techniques have been used from the vapor or the liquid phase [1, 10–12]. One promising alternative is the use of electrospinning combined with heat treatment to generate a nanofiber network film [5, 13–18]. This versatile technique has been broadly applied for solution processing of fibers from polymeric materials, as well as bioactive glass and ZnO, to name a few. For example, thermal processing electrospun polyacrylonitrile produced a high-purity carbon nanofiber web that was proposed as a potential anode for high-power lithium-ion batteries [13]. The control of morphology and fiber orientation in the electrospinning of the polymer precursor fiber has been addressed in numerous studies. Methods have been proposed and proven for controlling the fiber alignment: for instance the work by Dzenis [19]. However, thermal treatment parameters, such as calcination time, on the as-spun precursor fiber pattern and fiber diameter are still under investigation [18]. More recently, Kim et al. reported their results concerning the morphological variation because of several effects, and concluded that calcination conditions were the most significant factor [20].

The associated increase in surface area of nanoscale fillers offers advantageous electrical properties in polymeric composites, when compared to their bulk form and to traditional micron-size fillers [9, 21–23]. Polymer composites of high dielectric constant, for instance, are desirable for a variety of high dielectric constant electronic devices, such as transducers, piezo-sensors, hydrophones [24] and in producing electromagnetic antennas. Malmonge et al. [25]. produced flexible composites of poly(3-hydroxybutyrate) (PHB) and lead zirconium titanate (PZT) for ferroelectric and dielectric applications. They

Correspondence to: Melih Papila; e-mail: mpapila@sabanciuniv.edu  
Contract grant sponsor: The Scientific and Technological Research Council of Turkey—TÜBİTAK; contract grant number: Grant 106M364.  
DOI 10.1002/pc.20886  
Published online in Wiley InterScience (www.interscience.wiley.com).  
© 2009 Society of Plastics Engineers

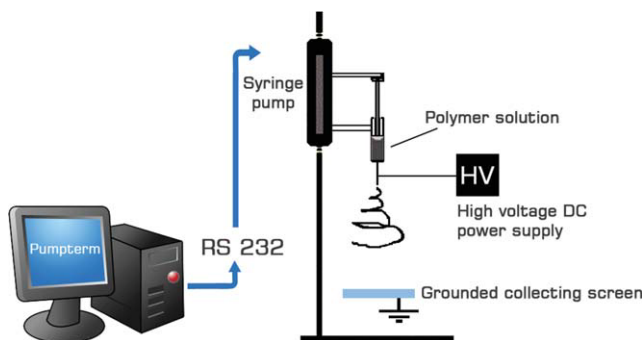


FIG. 1. Schematic representation of the computer-controlled electrospinning setup. [Color figure can be viewed in the online issue, which is available at [www.interscience.wiley.com](http://www.interscience.wiley.com).]

produced composites of different compositions and demonstrated the effect of PZT volume percentage. At a threshold ceramic content, the dielectric constant can increase the dielectric constant of PHB by as much as five times. It has also been noted that the composite properties depend on the size, geometry, and surface quality of the filler materials and could be tailored, if the dispersion of the fillers could be controlled [21, 26]. Hong et al. [21] studied the dielectric constant of a ZnO/LDPE composite and the effects because of the particle size and spatial distribution of the ZnO filler. Just recently, the effects of percolation and filler distribution morphology on the dielectric properties were reported by Wang et al. [22] for radial-ZnO/PVDF composites. Their results demonstrated that a significant increase in the dielectric constant was achieved by the addition of R-ZnO fillers into the polymer matrix, provided that the filler volume fraction remained below the percolation threshold.

The work being presented here introduces the concept of using electrospinning to form an inorganic filler network to secure the dispersion and distribution of the fillers in the polymer matrix. Specifically, we report on the feasibility of fibrous ZnO fillers by electrospinning and their insertion into PVDF polymer matrix to form the nanocomposite. The process for producing the fibrous-ZnO/PVDF nanocomposite is described in the next section, followed by the dielectric characterization of the nanocomposite under various frequency and temperature along with the crystalline structure. Supporting evidence for the results and associated discussions are provided by the x-ray diffractometry (XRD), scanning electron microscopy (SEM), and Raman spectroscopy.

## EXPERIMENTAL

The processing in the present work consists of two major stages: (1) the electrospinning of the polymer solution to form precursor fibers containing zinc; (2) thermal treatment of these fibers, i.e. calcination/sintering to form a fibrous ceramic structure. The process parameters, including solution concentrations, calcination temperature,

and exposure time were investigated independently, to achieve a continuous ZnO fibrous network.

### Electrospinning of Precursor Fibers

In a homemade electrospinning set-up, as depicted in Fig. 1, a polymer solution inserted into a syringe that has a 300  $\mu\text{m}$  diameter nozzle, was subjected to a DC bias ranging between 5 and 15 kV. The rate of the polymer flow from the syringe was determined by a computer controlled syringe pump (New Era NE-1000 Syringe Pump along with Pumpterm Software). Under the applied electric field, the polymer solution was extracted from the nozzle onto the collector due to high electrostatic force acting on the polymer droplet at the tip of the nozzle [27]. As the polymer jet traveled through air, a fiber was formed, and its diameter was reduced significantly by the solvent evaporation. The randomly oriented, fine fibers collected on the screen positioned above the collector plate produced a fiber mat, of a nano- to micron-scale determined by the process parameters.

Electrospun PVA fibers with a surface decorated by zinc acetate (ZnAc) particles were produced by electrospinning a PVA-ZnAc precursor solution [28, 29]. The precursor solution was prepared with PVA-distilled water (5:20 w/w) and Zn Acetate-distilled water (6:20 w/w) solutions separately. These two solutions were homogenized by stirring for 4 h. The viscous PVA solution was then poured into the ZnAc solution, which was then heated to 60°C and stirred for 5 h, to ensure a homogeneous distribution of the zinc and acetate ions. The solution was cooled to room temperature and then electrospun [3]. The electrospinning process was optimized for two process variables: voltage and distance between the syringe tip and the collector target. The best result for the production of a continuous and fine precursor fiber was obtained when the

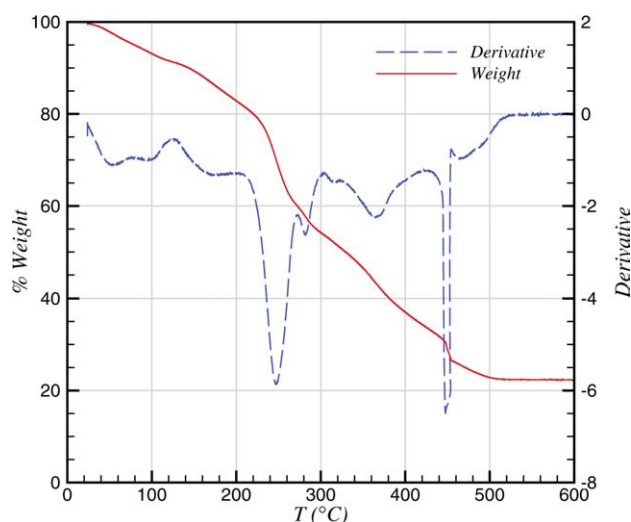


FIG. 2. TGA results showed that the inorganic part is attained after 450°C. [Color figure can be viewed in the online issue, which is available at [www.interscience.wiley.com](http://www.interscience.wiley.com).]

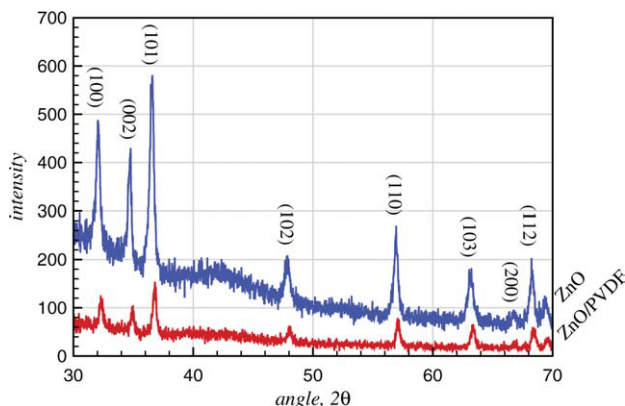


FIG. 3. In XRD spectra obtained from the ZnO fiber mat and fibrous-ZnO/PVDF composite samples, the peaks matched those of the wurtzite form of ZnO [24, 30, 31]. [Color figure can be viewed in the online issue, which is available at [www.interscience.wiley.com](http://www.interscience.wiley.com).]

applied voltage and the collector distance were 10 kV and 8 cm, respectively. The resultant electrospun mat exhibited a fibrous structure of PVA (with an average fiber diameter of 700 nm) onto which ZnAc particles were distributed.

#### Calcination and Sintering

To produce ZnO fibers, the next step was the thermal treatment of the precursor fiber mat, to eliminate the organics for producing ZnO (i.e. calcination) and sintering of the ZnO grains. The necessary thermal treatment schedule was determined via DTA/TGA simultaneous analysis. As seen from Fig. 2, the elimination of organic substances at 250, 360, and 450°C suggested that the organic burn-out was completed below 500°C. Because the weight loss was about 73% after calcination and Zn has a higher density than other atoms in the structure, the volume of the heat treated mat was significantly reduced. Therefore, the slow removal of the organics from the organic fiber mat was imperative. For this purpose, a stepwise heating schedule was applied with several ramp and dwell steps. With a heating ramp rate of 0.5°C/min, the dwell steps for calcination were held at 120, 300, 400, 500, and 600°C, each lasting ~12 h in duration. Sintering was carried out at 1200°C for an additional hundred hours. In total, ~9 days to obtain the ZnO fiber mat. This prolonged treatment allowed the successful removal of the organics and the formation of inorganic fibers formed from ZnO particles. The significant amount of shrinkage of the sample also implied that there would be friction between the surface of the platinum substrate and the sample during the heat treatment. Therefore, the organic mat was suspended over an intentionally wrinkled surface of the Pt-tray, to minimize the contact between the fibrous mat and the substrate.

#### Fibrous ZnO/PVDF Matrix Composite Formation

To manipulate the extremely fragile ZnO fiber mats and perform dielectric characterization, the electrospun fibrous

mat was carefully placed between two solution-cast polyvinylidene fluoride (PVDF) films and pressed at a temperature above the melting point of PVDF. The PVDF (Alfa Aesar) solution in dimethylformamide was first prepared 10% w/w at room temperature. The solution was then cast on a glass substrate kept in an oven, at 60°C for 4 h. Finally, to maintain the planar network of the ZnO fibers, the ZnO mat was sandwiched between the two PVDF solution-cast films and pressed to melt at 180°C. Upon cooling, a ZnO/PVDF flexible composite film was produced.

## RESULTS AND DISCUSSION

### Content, Crystalline Structure and Morphology

The first crucial assessment was to ascertain that the ZnO had remained intact in the resultant fibrous mat. The content of the mat was analyzed by energy-dispersive x-ray spectroscopy (EDXS) under a 15 kV and 6 mm working distance. EDXS results showed the signatures of Zn and O at weight fractions of 55% and 45%, respectively, and confirmed that the mat was made of fibrous ZnO.

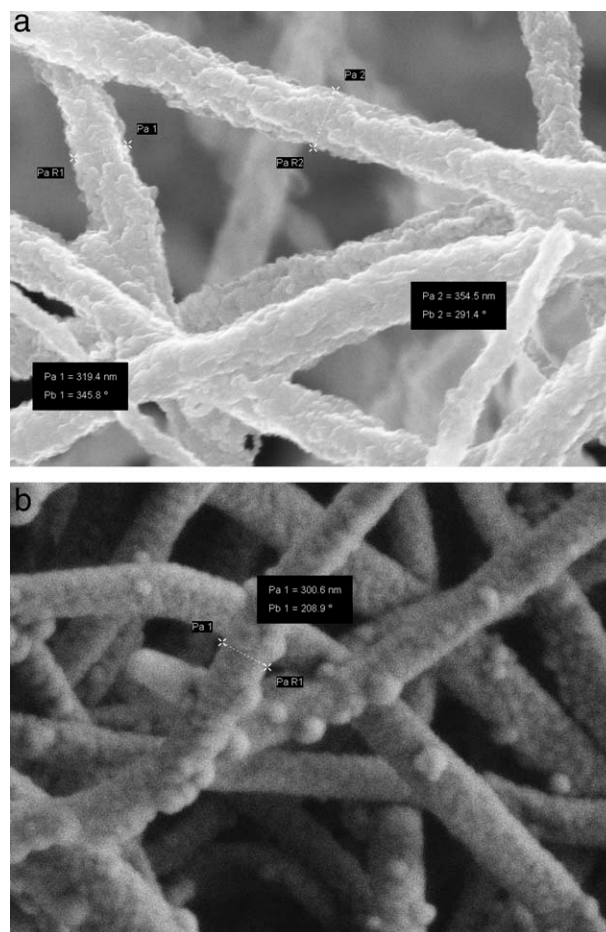


FIG. 4. SEM images of the ZnO fibers treated at (a) 600°C and (b) 1200°C.

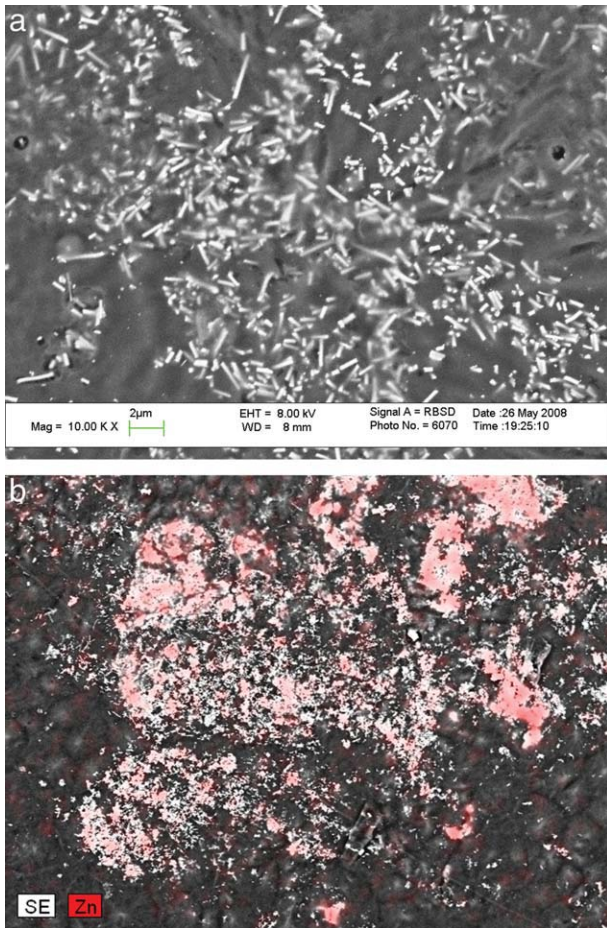


FIG. 5. Fibrous-ZnO/PVDF composite film (a) back-scattered SEM image, (b) EDX spectra obtained using a beam of 15kV accelerating voltage. [Color figure can be viewed in the online issue, which is available at [www.interscience.wiley.com](http://www.interscience.wiley.com).]

Next, the crystalline structure of the ZnO fiber mats was determined by XRD (Bruker AXS D8) measurements. The reflection angles coming from the specific crystal planes shown in Fig. 3 were consistent with that of the wurtzite form of ZnO [22]. This crystal structure is particularly important, since the electroactive characteristics of ZnO stem from the inherent symmetry [30, 32, 33].

The fibers and the mat heat-treated at 600°C were both extremely difficult to handle; whereas fibers sintered at 1200°C resulted in their somewhat improved handling and strength. A denser and well sintered morphology of the polycrystalline fibers and mats (see Fig. 4) were observed at 1200°C.

The fibrous-ZnO/PVDF composite was also characterized by XRD and SEM. The XRD spectra of the fibrous-ZnO/PVDF composite (see Fig. 3) were consistent with the peaks for the ZnO fiber mat. The SEM images of the composite (see Fig. 5) suggested that the high aspect ratio ZnO fragile fibers had been broken into short fibers (~2 μm in length) during the casting procedure. Moreover, the in-plane distribution and projection of the mat

appear to be maintained, and the ZnO fillers were well-dispersed in the PVDF matrix. Control of the aspect ratio and the volume fraction of the fillers (~10% in this work) was not in the scope of this article, but these factors and their effects in the composite properties are worth investigating in future studies. Nevertheless, the idea of using an inorganic filler network by electrospinning for the benefit of securing the dispersion of the fillers in the composite is considered to be a major contribution in this work. In addition, incorporating the fiber network into a hot-press-cast composite film enabled both handling and dielectric measurement.

### Dielectric Properties of the Fibrous-ZnO/PVDF Composite Film

This section presents dielectric measurements to determine the dielectric constant,  $\epsilon'$ , and the dielectric loss ( $\tan \delta = \epsilon''/\epsilon'$ ) of the PVDF and fibrous-ZnO/PVDF composite films. Dielectric properties of the samples were probed by using Hewlett-Packard 4194A Impedance/Gain-Phase Analyzer. Measurements per test temperature were taken

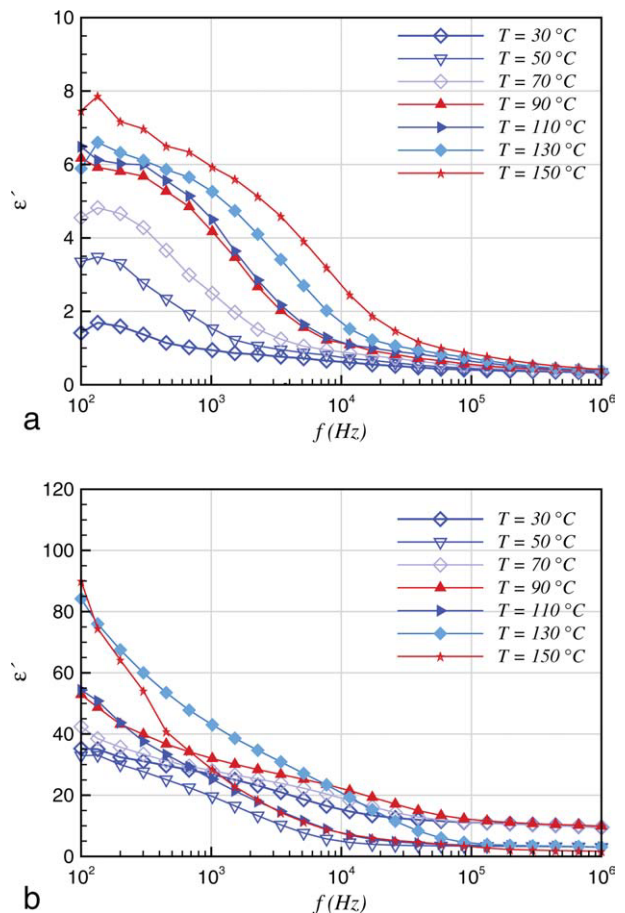


FIG. 6. Dielectric constant: frequency-temperature scan, (a) PVDF film obtained by melt pressing of a single-layer, solution-cast film, and (b) fibrous-ZnO/PVDF composite film. [Color figure can be viewed in the online issue, which is available at [www.interscience.wiley.com](http://www.interscience.wiley.com).]

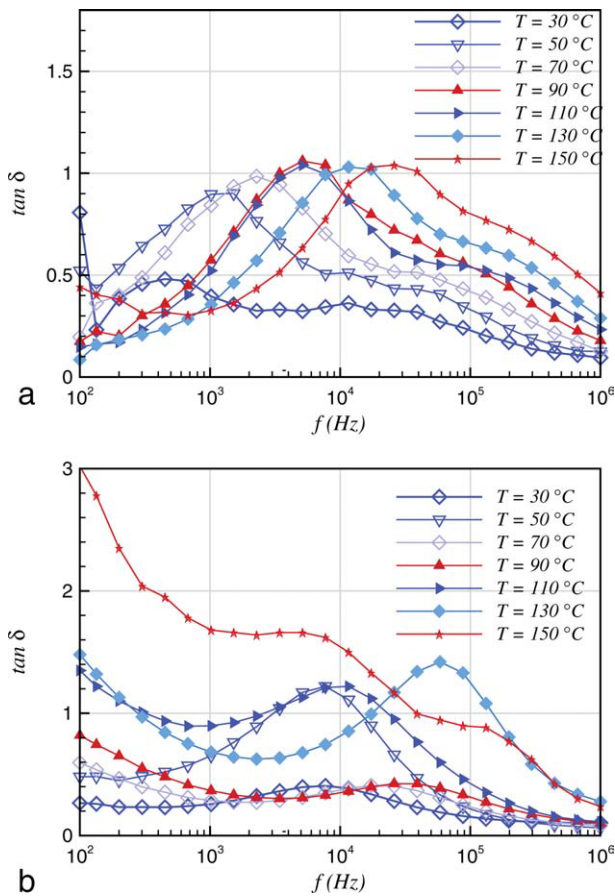


FIG. 7. Dielectric loss: frequency-temperature scan (a) PVDF film obtained by melt pressing of a single-layer, solution-cast film, and (b) fibrous-ZnO/PVDF composite film. [Color figure can be viewed in the online issue, which is available at [www.interscience.wiley.com](http://www.interscience.wiley.com).]

between 100 Hz and 1 MHz, while the temperature scan was made from 30 to 150 °C at every increment of 10 °C. The measurement system used a PT 100 resistor in direct thermal contact with the sample, providing accuracy better than 0.1 °C, by using the NOVOTHERM Temperature Control Unit. The time for each frequency sweep was  $\sim$ 1 min. Alternating current dielectric properties were analyzed by monitoring the capacitance and conductivity. For each temperature, the real and imaginary part was recorded for the dielectric permittivity as well as time, temperature and frequency.

The dielectric constant or relative permittivity  $\epsilon'$  (measure of stored polarization energy) of the PVDF cast film and the fibrous-ZnO/PVDF composite film had changed as the frequency and temperature were varied. The relevant frequency-temperature scans for the two films are presented in Fig. 6. The behavior of the dielectric constant is qualitatively similar. In particular, a comparison of the low frequency versus high frequency response, revealed that the relative permittivity  $\epsilon'$  decayed as the frequency was increased. Moreover, quantitative comparison of the two films, ZnO/PVDF composite vs. the PVDF specimen, showed a substantial increase by a factor of 10,

over all frequency-temperature settings for the composite (Fig. 6a vs. b).

The polarization mechanism driving the measured dielectric behavior of the fibrous-ZnO/PVDF composite was thought to be the interfacial polarization jump for two reasons. The first was because of the fact that the other three mechanisms—electronic, ionic, and molecular or dipolar—typically impart polarization relaxations or resonance as observed, but at much higher frequencies [31, 34] than were scanned. Second, by creating the large amounts of submicron filler/polymer interfacial area, the dielectric behavior was enhanced, as shown in Fig. 6b, when compared to the dielectric constant measured on a bulk ZnO/PVDF composite [22, 23]. With comparable ZnO volume fractions at  $\sim$ 10%, the dielectric constant of the fibrous-ZnO/PVDF composite (near 30 at 100 Hz) was twice that of the bulk-ZnO/PVDF composite ( $\sim$ 14.0 maximum at room temperature and 100 Hz), as reported by Wang et al. [22]. This enhancement in dielectric

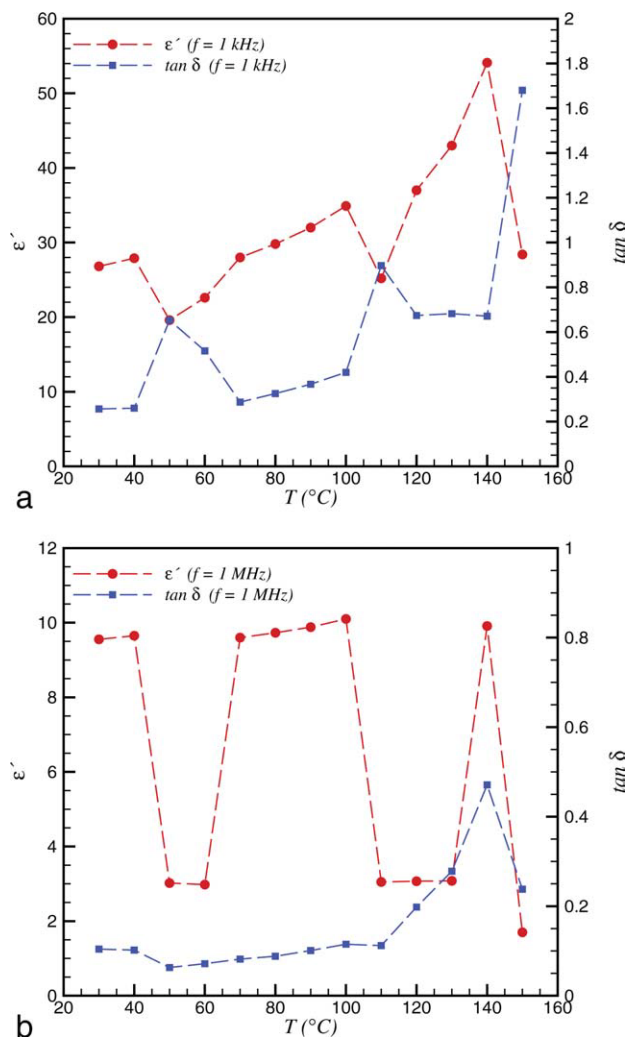


FIG. 8. Temperature effect on the dielectric constant and loss of the fibrous-ZnO/PVDF composite: (a) at 1 kHz and (b) at 1 MHz. [Color figure can be viewed in the online issue, which is available at [www.interscience.wiley.com](http://www.interscience.wiley.com).]

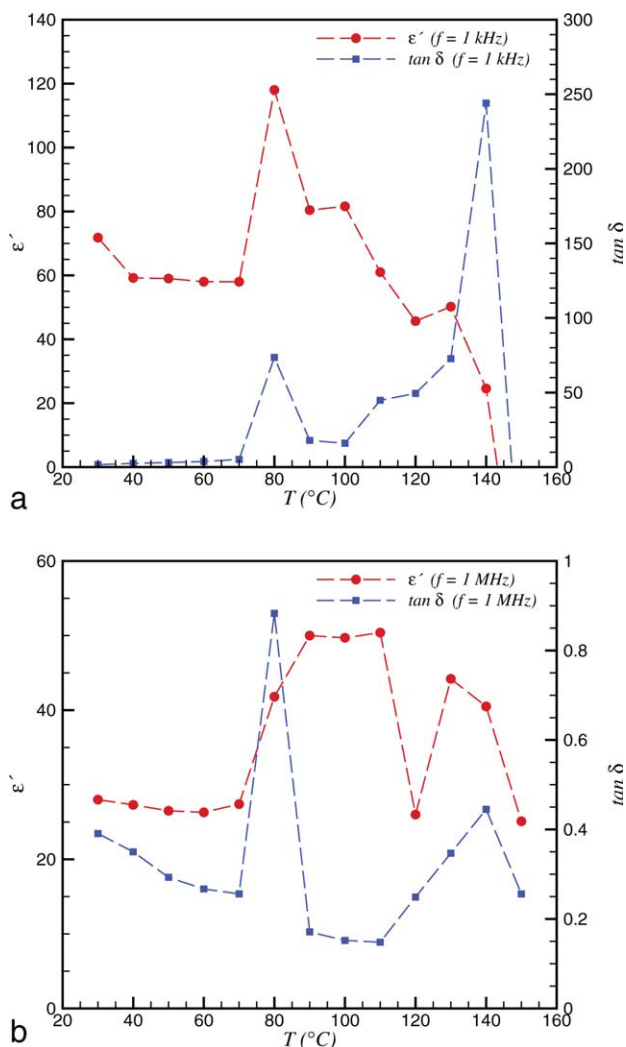


FIG. 9. Temperature effect on the dielectric constant and loss of ZnOH (a) at 1 kHz and (b) at 1 MHz. [Color figure can be viewed in the online issue, which is available at [www.interscience.wiley.com](http://www.interscience.wiley.com).]

behavior could be attributed to the ceramic/polymer interfaces acting as effective blocking barriers, since they limit the charge carrier motion and give rise to interfacial polarization [35, 36], which was further evidenced by the increase in permittivity with decreasing frequency [21]. Furthermore, the internal interfaces (e.g., grain boundaries) of the polycrystalline ZnO fibers also contributed dielectric polarization [24, 35, 37]. Different polarizabilities along different crystallographic directions occurred, depending on the orientation of crystallites forming the electrospun/sintered fiber.

Another salient property of a dielectric is the ability to support an electrostatic field, while dissipating minimal energy in the form of heat. A lower dielectric loss (the proportion of energy lost as heat) suggests a more effective dielectric material. By considering the loss tangent, which is the ratio of energy dissipated to energy stored, the overall dissipation factor could be determined, as shown in Fig. 7 for both films. Despite the differences

between the magnitude of stored energy for PVDF and ZnO/PVDF composite films, the loss tangent for both films remained in the same scale. The qualitative behavior, on the other hand, differed, manifested by a shift to higher frequencies in the polarization relaxation associated with the dielectric loss, as also observed by Park et al. [38]. Moreover, the dielectric loss tends to increase at elevated temperatures in Fig. 7.

Closer inspection of the spectra in Figs. 6 and 7 reveals that the effect of temperature on the real part of the dielectric constant  $\epsilon'$ , of fibrous-ZnO/PVDF composite did not impart a regular trend. The irregularity or anomaly could be seen more clearly on plots of  $T$  vs.  $\epsilon'$  and  $T$  vs  $\tan \delta$  for specific test frequencies, as reflected by the data collected at 1 kHz and 1 MHz (see Fig. 8). The stable dielectric properties appeared in the range of 60–100 $^{\circ}\text{C}$ . The deviation or discontinuities on the otherwise regular, trend-like behavior occurred in the 40–60 $^{\circ}\text{C}$  range, and at elevated temperatures above 100 $^{\circ}\text{C}$ . Note that a similar plot was also reported by Hong et al. [21], for the ZnO/LDPE composite, showing a similar monotonic increase of the dielectric constant from room temperature up to 100 $^{\circ}\text{C}$ , albeit lacking measurements at 50, 60, and 90 $^{\circ}\text{C}$ .

The dielectric constant of the composite is built up by the contributions of both PVDF and ZnO. Because of discontinuities at elevated temperatures, particularly above 90 $^{\circ}\text{C}$ , one may suspect that the moisture uptake of the composite could affect the dielectric response of the material. Because of the large surface area and high surface energy of the ZnO filler, the fibers could be absorbing more target molecules, thereby producing hydroxyl radicals [33]. Another possibility would be the formation of surface defects on ZnO nanostructures and associated OH groups at the surface after thermal treatment [39]. Both possibilities, the moisture uptake of the composite and defects driven surface chemistry of the ZnO, point to the

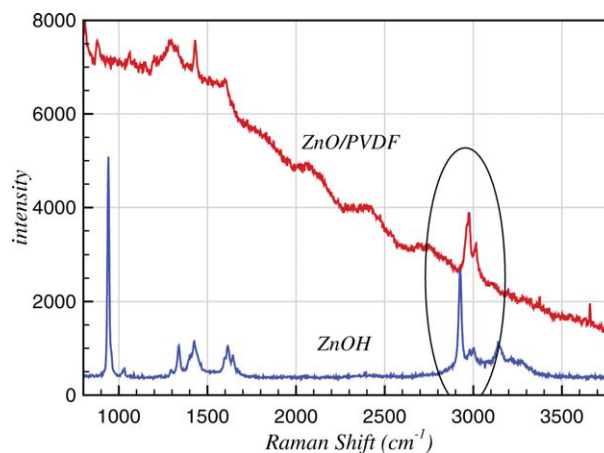


FIG. 10. Raman Spectra of the fibrous-ZnO/PVDF composite and ZnOH samples in the range of 800–3800  $\text{cm}^{-1}$ . [Color figure can be viewed in the online issue, which is available at [www.interscience.wiley.com](http://www.interscience.wiley.com).]

OH groups or radicals as the potential cause for the anomalies when temperature varies. Furthermore, the sudden drop in the dielectric constant was observed beyond 140°C. A similar drop was also observed by Wang et al. [22] for their ZnO/PVDF and by Dang et al. [40] for BaTiO<sub>3</sub>/PVDF composite specimens, which was attributed to the thermal expansion and subsequent softening of the polymer matrix PVDF as its melting starts at about 130°C.

To evaluate the anomaly or decrease of the dielectric constant around 50–60°C and at around 100°C, and whether they are OH-groups related, frequency-temperature scans were also performed on a pellet specimen of ZnOH prepared from a ZnAc and NH<sub>4</sub>OH solution. Figure 9 shows the ZnOH dielectric behavior as a function of temperature at 1 kHz and 1 MHz. The dielectric constant decreased at ~50 and 60°C. As the temperature increased, the fluctuating values were attributed to the increased OH movements, generating more OH/OH interface in the ZnOH. After 90°C, the steep increase of the dielectric constant appeared to stop and sharply drop at 110°C. Changes between 90 and 120°C were caused by moisture removal from the specimen. Fluctuations in the fibrous-ZnO/PVDF composite film could also be attributed to the OH groups, which appear to be common in the composite and the ZnOH specimens. Note that a higher dissipation was observed in the ZnOH sample than in fibrous-ZnO/PVDF composite because of higher fraction of the OH groups in ZnOH and associated movements. The existence or sign of OH groups was additionally confirmed by Raman spectroscopy (see Fig. 10), which showed peaks for the stretching mode of the OH groups in the anticipated range of 2800–3600 cm<sup>-1</sup> [41].

## CONCLUSIONS

A poly(vinyl alcohol)-zinc acetate solution was electrospun to produce randomly oriented precursor polymeric fiber mats. The precursor mats were subjected to a controlled thermal treatment (calcination and sintering) to form the ZnO fibrous structures. The mechanical drawback of the ZnO fibrous mat, being extremely fragile, was circumvented by first sandwiching the mat between solution cast PVDF films and then making a polymer matrix-composite via hot-press melt casting.

The use of an inorganic filler network by electrospinning for the benefit of securing the dispersion of the fillers in the composite was herein originally introduced and demonstrated. The network of high aspect ratio fibrous ZnO had been altered during the melt casting, and ZnO short fibers of nanoscale diameter in the PVDF matrix were obtained instead. The in-plane distribution of the ZnO fillers (short fibers) in the PVDF matrix appears to comply with the projection of the pristine ZnO mat before hot-pressing.

Moreover, the proposed process flow for the fibrous-ZnO/PVDF flexible composite facilitated handling and

enabled measurements for dielectric properties, not practical on a ZnO fibrous mat. The ZnO short fibers of high surface area and their polycrystalline morphology allowed the generation of interfacial polarization, because of both the increase in dipoles formed at ZnO/PVDF interface, and at internal interfaces in the fibers of the composite film. The enhanced interfacial polarization had significantly increased the dielectric response over the bulk properties of both constituents, as well as over bulk-ZnO/PVDF, albeit with a slight penalty on dielectric loss was measured. Increasing temperatures and decreasing frequencies have elevated the dielectric constant of the ZnO/PVDF composite. The stable dielectric properties appeared in the range of 60–100°C. The observed temperature dependence and instabilities were attributed to OH groups in the fibrous-ZnO/PVDF composite.

## ACKNOWLEDGMENTS

This manuscript is an extended version of the article presented at “Nanocomposites: Electrical and Thermal 1A” session of SAMPE08 Fall Technical Conference, “Multifunctional Materials: Working Smarter Together”, held in Memphis, USA Sep 8–11, 2008.

## REFERENCES

1. S. Roy and S. Basu, *Bull. Mater. Sci.*, **25**(6), 513 (2002).
2. Q. Zhang, T.P. Chou, B. Russo, S.A. Jenekhe, and G. Cao, *Adv. Funct. Mater.*, **18**, 1654 (2008).
3. B. Pal and M. Sharon, *Mater. Chem. Phys.*, **76**, 82 (2002).
4. C.X. Xu, X.W. Sun, B.J. Chen, and P. Shum, *J. Appl. Phys.*, **95**, 661 (2004).
5. P. Viswanathamurthi, N. Bhattarai, H. Y. Kim, and D.R. Lee, *Nanotechnology*, **15**, 320 (2004).
6. P.M. Martin, M.S. Good, J.W. Johnston, L.J. Bond, and J.D. Lin, *Thin Solid Films*, **379**, 253 (2000).
7. Z. Qifeng, P.C. Tammy, R. Bryan, A.J. Samson, and C. Guozhong, *Adv. Mater.*, **18**, 11 (2008).
8. L.W. Zhang, Y.K. Xiang, D. Yang, G. Puxian, L.H. William, Y. Rusen, and Z. Yue, *Adv. Mater.*, **14**, 10 (2004).
9. M.H. Zhao, Z.L. Wang, and S.X. Mao, *Nano Lett.*, **4**(4), 587 (2004).
10. P.X. Gao and Z.L. Wang, *J. Appl. Phys.*, **97**, 044304 (2005).
11. Y.C. Wang, I.C. Leu, and M.H. Hon, *Electrochem. Solid State Lett.*, **5**(4), C53 (2002).
12. Y. Li, G.W. Meng, L.D. Zhang, and F. Philipp, *Appl. Phys. Lett.*, **76**, 2011 (2001).
13. C. Kim, K. Yang, M. Kojima, K. Yoshida, Y.J. Kim, Y. Kim, and M. Endo, *Adv. Funct. Mater.*, **16**, 2393 (2006).
14. H.W. Kim, E. Kim, and J.C. Knowles, *Adv. Funct. Mater.*, **16**, 1529 (2006).
15. I.S. Chronakis, *J. Mater. Process. Technol.*, **167**, 283 (2005).
16. W. Sigmund, J. Yuh, H. Park, V. Maneeratana, G. Pyrgiotakis, A. Daga, J. Taylor, and J. C. Nino, *J. Am. Ceram. Soc.*, **89**(2), 395 (2006).

17. Y. Wang, M. Aponte, N. Leon, I. Ramos, R. Furlan, and N. Pinto, *J. Am. Ceram. Soc.*, **88**(8), 2059 (2005).
18. H. Wu and W. Pan, *J. Am. Ceram. Soc.*, **89**, 699 (2006).
19. Y.A. Dzenis, *Science*, **304**, 1917 (2004).
20. Y. Kim, D.Y. Lee, M.H. Lee, N.I. Cho, Y.S. Song, and S.J. Lee, *J. Korean Phys. Soc.*, **53**, 421 (2008).
21. J.I. Hong, P. Winberg, L.S. Schadler, and R.W. Siegel, *Mater. Lett.*, **59**, 473 (2005).
22. G. Wang, Y. Deng, Y. Xiang, and L. Guo, *Adv. Funct. Mater.*, **18**, 1 (2008).
23. T.J. Lewis, *IEEJ Trans. Fundam. Mater.*, **126**(11), 1020 (2006).
24. C.K. Chiang and R. Popielarz, *Ferroelectrics*, **275**, 1 (2002).
25. J.A. Malmonge, L.F. Malmonge, G.C. Fuzari Jr., S.M. Malmonge, and W.K. Sakamoto, *Polym. Compos.*, (2008).
26. L. Flandin, M. Verdier, B. Boutherin, Y. Brechet, and J.Y. Cavaille, *J. Polym. Sci. Part B: Polym. Phys.*, **37**, 805 (1999).
27. L. Dan and X. Younan, *Adv. Mater.*, **16**, 14 (2004).
28. O.S. Yordem, Piezoelectric Ultrafine Polymer and Ceramic Fibers By Electrospinning: Process Development and Characterization. MSc Thesis, Sabanci University, Istanbul, Turkey (2006).
29. O.S. Yordem, M. Gülleroğlu, E. Öğüt, Y.Z. Menciloğlu, M. Papila, Piezoelectric Polymer and Ceramic Ultrafine Fibers for Piezocomposite Films in *Proceedings of the 21st Annual Technical Conference, American Society for Composites, Dearborn MI* 2006.
30. F. Lu, W. Cai, and Y. Zhang, *Adv. Funct. Mater.*, **18**, 1047 (2008).
31. H. Foll. Electronic materials, lecture notes, U.of Kiel, available at [http://www.tf.uni-kiel.de/matwis/amat/elmat\\_en/index.html](http://www.tf.uni-kiel.de/matwis/amat/elmat_en/index.html), last accessed on September 17, (2008).
32. X. Zhiyong, H. Jiann-Yang, L. Bowen, H. Xiaodi, and W. Howard, *J. Occup. Med.*, **60**, 29 (2008).
33. R.Y. Hong, L.L. Chen, J.H. Li, H.Z. Li, Y. Zheng, and H. Ding, *J. Polym. Adv. Technol.*, **18**, 901 (2007).
34. J. Xu and C. P. Wong, *J. Electron. Mater.*, **35**(5), 1087 (2006).
35. J.-C. M'Peko, *J. Mater. Sci. Lett.*, **19-21**, 1925 (2000).
36. R.V. Rao and M. H. Shridhar, *Mater. Lett.*, **55**, 34 (2002).
37. F. Bernardini and V. Fiorentini, *Phys. Rev. B*, **57**, 16 (1997).
38. S.H. Park, E.C. Lim, K.S. Park, D.H. Kang, S.O. Han, and D.C. Lee, The Dielectric Properties of Functional PVDF thin films by Physical Vapor Deposition Method in *Proceedings of the 5th International Conference on Properties and Applications of Dielectric Materials* Seoul, Korea, May 25–30 (1997).
39. A.B. Djuricic, Y.H. Leung, K.H. Tom, Y.F. Hsu, L. Ding, W.K. Ge, Y.C. Zhong, K.S. Wong, W.K. Chan, H.L. Tom, K.W. Cheah, W.M. Kwok, and D.L. Phillips, *Nanotechnology*, **18**, 095702 (2007).
40. Z.M. Dang, J.B. Wu, L.Z. Fan, and C.W. Nan, *Chem. Phys. Lett.*, **376**, 389 (2003).
41. H. Zhou, H. Alves, D.M. Hofmann, B.K. Meyer Kaczmarczyk, A. Hoffmann, and C. Thomsen, *Phys. Status Solidi*, **229**(2), 825–828 (2002).